1

Remote sensing of the atmosphere

Climate change, stratospheric ozone depletion, tropospheric ozone enhancement, and air pollution have become topics of major concerns and made their way from the scientific community to the general public as well as to policy, finance, and economy (Solomon et al., 2007). In addition to these atmospheric changes related to human activities, natural events such as volcanic eruptions or biomass burning have a significant impact on the atmosphere, while the demands and expections on weather forecasting are steadily increasing (Chahine et al., 2006). Furthermore, the discovery of extrasolar planets with the possibility of hosting life (Des Marais et al., 2002) has brought a new momentum to the subject of planetary atmospheres.

In view of all these developments, atmospheric science comprising various fields of physics, chemistry, mathematics, and engineering has gained new attraction. Modeling and observing the atmosphere are keys for the advancement of our understanding the environment, and remote sensing is one of the superior tools for observation and characterization of the atmospheric state.

In this chapter a brief introduction to atmospheric remote sensing will be given. After a short survey of the state of the atmosphere and some of its threats, the atmospheric sounding using spectroscopic techniques is discussed. A review of the radiative transfer in (Earth's) atmosphere and a general characterization of atmospheric inverse problems will conclude our presentation.

1.1 The atmosphere – facts and problems

The state of planetary atmospheres, i.e., its thermodynamic properties, composition, and radiation field, varies in space and time. For many purposes it is sufficient to concentrate on the vertical coordinate and to ignore its latitude, longitude, and time-dependence. Various altitude regions of the atmosphere are defined according to the temperature structure: troposphere, stratosphere, mesosphere, and thermosphere (Figure 1.1).

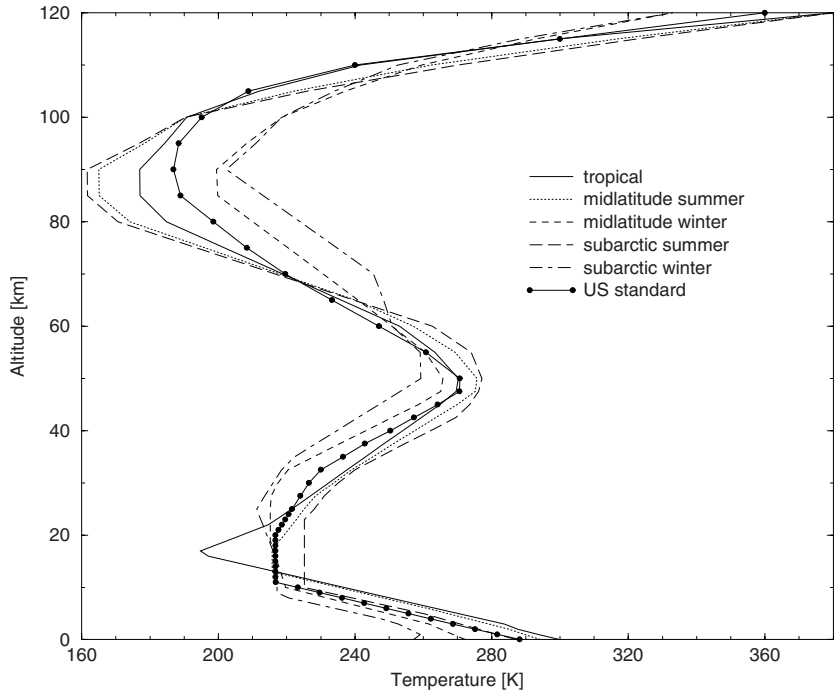

Fig. 1.1. AFGL (Air Force Geophysics Laboratory) reference-atmospheric models: temperatures (Anderson et al., 1986). The circles attached to the US standard profile indicate the altitude levels.

Pressure p decreases monotonically with increasing altitude z; according to the ideal gas law $p = nk_{\mathrm{B}}T$ and the hydrostatic equation $\mathrm{d}p = -g\rho\,\mathrm{d}z$ we have

$$p(z) = p_0 \exp\left(-\int_0^z \frac{\mathrm{d}z}{\bar{H}}\right).$$

Here, n is the number density, g is the gravity acceleration constant, k_{B} is the Boltzmann constant, $\rho = mn$ is mass density, and m is the mean molecular mass ($m \approx 29\,\mathrm{amu} = 4.82 \cdot 10^{-23}\,\mathrm{g}$ for dry air in Earth's lower and mid atmosphere). Ignoring the altitude-dependence of the factors defining the scale height

$$H(z) = \frac{k_{\mathrm{B}}T\,(z)}{mg},$$

yields

$$p\,(z) = p_0 \exp\left(-\frac{z}{\bar{H}}\right), \tag{1.1}$$

where p_0 is the surface pressure ($p_0 = 1\,\mathrm{bar} = 1013.25\,\mathrm{mb}$ for standard STP). Then, assuming a mean atmospheric temperature $T = 250\,\mathrm{K}$, gives the scale height $\bar{H} = 7.3\,\mathrm{km}$.

The terrestrial atmosphere is composed of a large number of gases and various solid and liquid particles (hydrometeors and aerosols), see Figure 1.2. The water- and aerosol-free atmosphere is made up of nitrogen (N_2, 78%) and oxygen (O_2, 21%) with almost constant mixing ratios in the lower and middle atmosphere. Water is present in all three phases

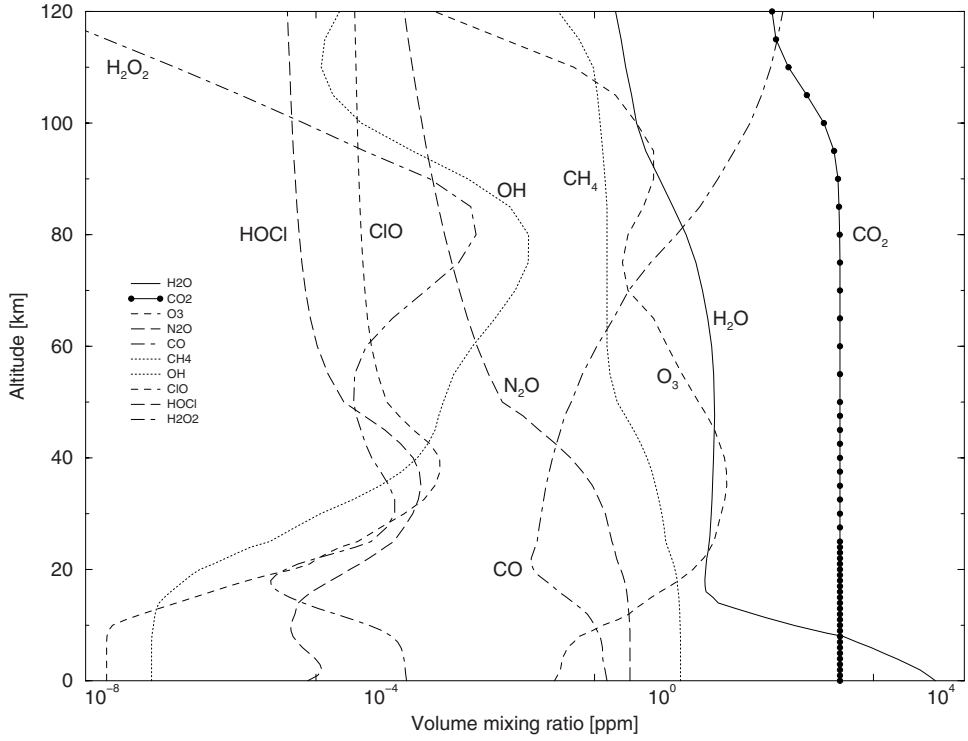

Fig. 1.2. AFGL reference atmospheric models: volume mixing ratios of selected molecules (Anderson et al., 1986).

(vapor, liquid droplets, and ice crystals) and varies significantly in space and time. The remaining 1% of the atmospheric gases are noble gases (0.95%) and trace gases (0.05%). The trace gases, which are mainly carbon dioxide, methane, nitrous oxide and ozone, have a large effect on Earth's climate and the atmospheric chemistry and physics.

Precise knowledge of the distribution and temporal evolution of trace gases and aerosols is important in view of the many challenges of the atmospheric environment.

1.1.1 Greenhouse gases

The greenhouse gases (carbon dioxide CO_2, methane CH_4, tropospheric ozone O_3, chlorofluorocarbons and to a lesser extent water H_2O) are responsible for Earth's natural greenhouse effect which keeps the planet warmer than it would be without an atmosphere. These gases block thermal radiation from leaving the Earth atmosphere and lead to an increase in surface temperature. In the last century, the concentration of greenhouse gases increased substantially: CO_2 from its pre-industrial level of about 280 ppm by more than 30% due to combustion of fossil fuels, and CH_4 by even more than 100%. As a consequence, one expects an average global warming of about $2°$C to $4°$C in the coming century. Hence, substantial changes of the environment can be expected with significant effects for the existing flora and fauna (Solomon et al., 2007).

1.1.2 Air pollution

Pollutants from natural processes and human activities like NO_2 and CO are emitted into the troposphere. In the northern hemisphere, the main source of pollutants is fossil fuel combustion coupled with some biomass burning, while in the southern hemisphere, biomass burning is the primary source. Acid rain produces severe damage to forests and aquatic life, especially in regions with a lack of natural alkalinity. This forms when SO_2 and NO_2 build up in the atmosphere. Sulfur dioxide and nitrogen dioxide are oxidized by reaction with the hydroxyl radical and generate sulfuric acid and nitric acid, respectively. These acids with a pH normally below 5.6 are then removed from the atmosphere in rain, snow, sleet or hail. It should be pointed out that the release of SO_2 into the atmosphere by coal and oil burning is at least two times higher than the sum of all natural emissions.

1.1.3 Tropospheric ozone

Ozone is a toxic and highly oxidizing agent. Photochemical ozone production in the troposphere, also known as summer smog, produces irritation of the respiratory system and reduces the lung function. The majority of tropospheric ozone formation occurs when nitrogen oxides, carbon monoxide and volatile organic compounds react in the atmosphere in the presence of sunlight. High concentrations of ozone arise when the temperature is high, humidity is low, and air is relatively static, and when there are high concentrations of hydrocarbons.

1.1.4 Stratospheric ozone

While ozone behaves like a greenhouse gas in the troposphere, in the stratosphere it helps to filter out the incoming ultraviolet radiation from the Sun, protecting life on Earth from its harmful effects. It is produced from ultraviolet rays reacting with oxygen at altitudes between 20 and 50 km, where it forms the so-called stratospheric ozone layer. In the upper stratosphere, ozone is removed by catalytic cycles involving halogen oxides. In addition, a very substantial depletion of stratospheric ozone over Antarctica and the Arctic has been observed during springtime. The main source of the halogen atoms in the stratosphere is photodissociation of chlorofluorocarbon compounds, commonly called freons, and of bromofluorocarbon compounds known as halons. These compounds are transported into the stratosphere after being emitted at the surface from industrial production. The loss of ozone in the stratosphere is also affected, in a synergistic manner, by the tropospheric emission of greenhouse gases.

1.2 Atmospheric remote sensing

Remote sensing means that measurements are performed at a large distance from the object or the medium to be investigated. The interaction of electromagnetic or acoustic waves with the medium is determined by the state of the medium, and the modification of the waves can be used for the retrieval of the medium's properties. The following discussion

concentrates on measurements of the electromagnetic radiation, but the mathematical tools for the solution of the inverse problem can equally well be applied to acoustic measurements, e.g., SONAR (SOund NAvigation and Ranging) or SODAR (SOund Detection And Ranging).

Remote sensing can be passive or active. Active remote sensing utilizes an artificial radiation source such as a laser emitting light pulses; the laser light is scattered by gas molecules and aerosols and it is partially absorbed by the target gas. A portion of the emitted light is collected by a detector telescope, and the analysis of the recorded laser light reveals information about the composition of the atmosphere. In LIDAR (LIght Detection And Ranging) systems, the transmitter and the detector are usually co-located and the technique is based on backscattering. Radar (radio detection and ranging) systems employ a similar technique using microwave-emitting antennas.

In contrast, passive remote sensing utilizes natural radiation sources. The observation of short-wave solar radiation propagating through the atmosphere, interacting with its constituents and partly being reflected by Earth's surface, and the observation of long-wave thermal emission of both atmosphere and surface are the main approaches. Passive remote sensing can be achieved by analyzing absorption or emission spectra as follows:

(1) Thermal emission. Instruments based upon the emission technique detect the long-wave radiation (infrared or microwave) thermally emitted in the atmosphere along the observer's line-of-sight. The signals from atmospheric constituents can be regarded as thermal 'fingerprints' of the atmosphere, and from the emission line properties, temperature or trace gas concentrations are derived.
(2) Absorption of solar radiation. The upwelling radiation at the top of the atmosphere from the ultraviolet to the near-infrared comprises the solar radiation that has been scattered by air molecules and aerosols, partially absorbed by the target gas and reflected at the Earth's surface. Information on trace gas concentrations is encapsulated in that part of the incoming solar radiation that has been removed by absorption.
(3) Absorption of direct radiation. This category includes occultation instruments that measure solar, lunar, and even stellar radiation directly through the limb of the atmosphere during Sun, Moon and star rise and set events. By measuring the amount of absorption of radiation through the atmosphere, occultation instruments can infer the vertical profiles of trace gas constituents.

A further classification of remote sensing systems is based on the sensor location and the observation geometry (Figure 1.3):

(1) Ground-based systems deployed in laboratory buildings usually observe the atmosphere in an 'uplooking' geometry. Observatories in mountain regions are frequently used with altitudes up to several kilometers, for example, in the Network for Detection of Atmospheric Composition Change (NDACC).
(2) Airborne remote sensing systems work with instruments onboard of aircraft or balloons. Whereas conventional aircraft operate in altitudes more or less confined to the troposphere, some aircraft such as the American ER-2 or the Russian Geophysica can reach altitudes of about 20 km, well in the lower stratosphere. Stratospheric balloons can reach altitudes of almost 40 km, hence permitting observation of the atmosphere in 'limb sounding' geometry.

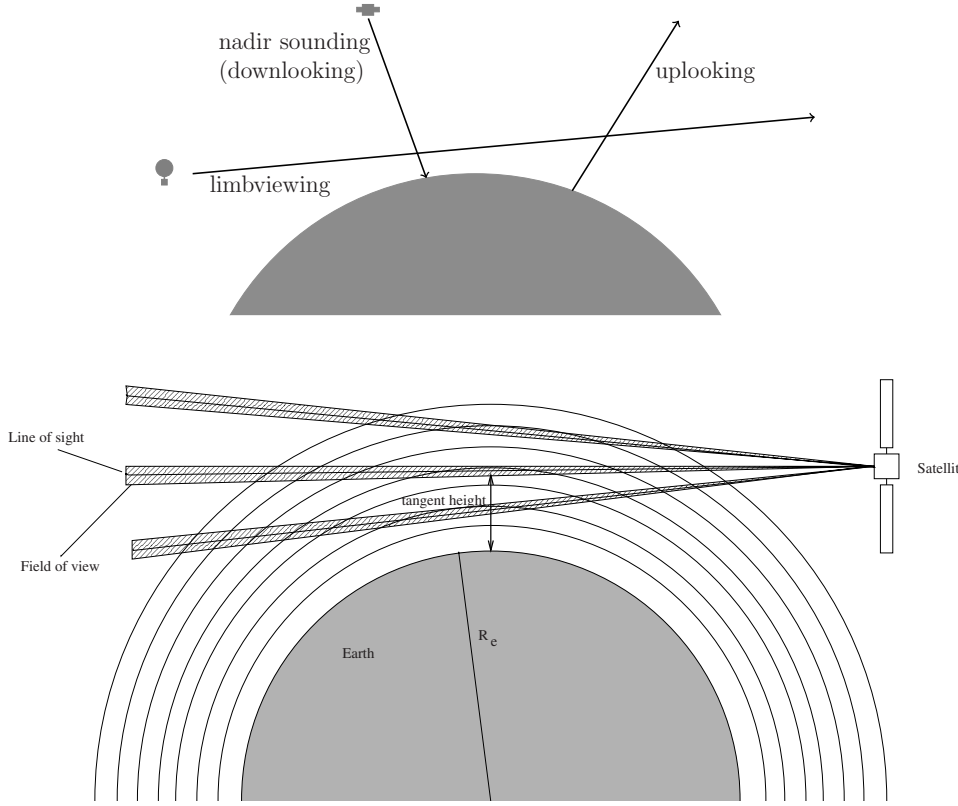

Fig. 1.3. Observation geometries for atmospheric remote sensing.

(3) Spaceborne systems aboard satellites, the Space Shuttle, or the International Space Station (ISS) work in limb viewing or in nadir viewing (downlooking) mode. A large number of sensors for environmental and meteorological studies is mounted on polar orbiting satellites flying at altitudes of about 800 km. Furthermore geostationary satellites with an altitude of about 36 000 km are utilized, especially for meteorological purposes. In contrast, Space Shuttles and the ISS are orbiting at altitudes of about 400 km or less.

Figure 1.4 illustrates the incoming extraterrestrial solar radiation at the top of the atmosphere (TOA) versus wavelength. It is noted that for solar wavelengths beyond 1.4 μm the solar emission curve closely resembles a blackbody radiator having a temperature of about 6000 K. The lower curve depicts a MODTRAN4 (MODerate resolution atmospheric TRANsmission) calculation (Berk et al., 1989) for the downwelling solar flux density reaching the ground. The solar zenith angle has been set to 60°, while for the composition and state of the atmosphere a midlatitude summer case has been adopted. All relevant absorbing atmospheric trace gases, as shown in the figure, were included in the radiative transfer computation which had a moderate spectral resolution of about 20 cm^{-1}. Similarly, in Figure 1.5 we show the infrared spectrum of the Earth atmosphere. The results

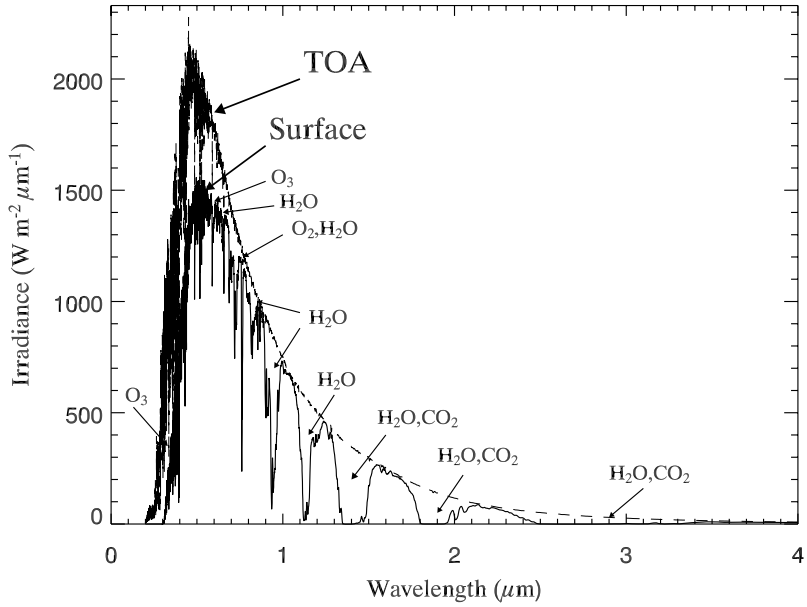

Fig. 1.4. Spectral distribution of the incoming solar flux density at the top of the atmosphere (TOA) and at ground level for a clear sky atmosphere and a nonreflecting ground. The solar zenith angle has been set to 60°. (Adapted from Zdunkowski et al. (2007).)

correspond to a clear sky US standard atmosphere and are also computed with the radiative transfer band model MODTRAN4. Figures 1.4 and 1.5 clearly demonstrate that UV and IR spectra of the terrestrial atmosphere contain a wealth of information about its state, and, in particular, signatures of a large number of molecular absorbers can be identified. Two examples will serve to illustrate the basic principles of atmospheric remote sensing.

In the UV wavelength range 290–330 μm, not only do spaceborne nadir observations of the radiance enable determination of the total column amount of ozone below the subsatellite point but scanning from smaller to larger wavelengths also allows us to 'sound' the atmosphere as a function of increasing distance from the sensor. Ozone molecules absorb solar radiation strongly at short wavelengths, i.e., photons entering the atmosphere are not able to penetrate the ozone layer in the stratosphere (with maximum concentration around 20 or 25 km). On the other hand, photons with higher wavelengths have a better chance to reach a greater depth (lower altitude) before they are absorbed.

Weather forecasting heavily relies on sounding of the atmospheric temperature profile using satellite observations in the infrared or microwave region following the pioneering work of King and Kaplan. King (1956) showed that the vertical temperature profile can be estimated from satellite radiance scan measurements. Kaplan (1959) demonstrated that intensity measurements in the wing of a CO_2 spectral band probe the deeper regions of the atmosphere, whereas observations closer to the band center see the upper part of the atmosphere. Analogously, the complex of O_2 lines in the microwave spectral range can be used. In both cases one utilizes emission from a relatively abundant gas with known and uniform distribution.

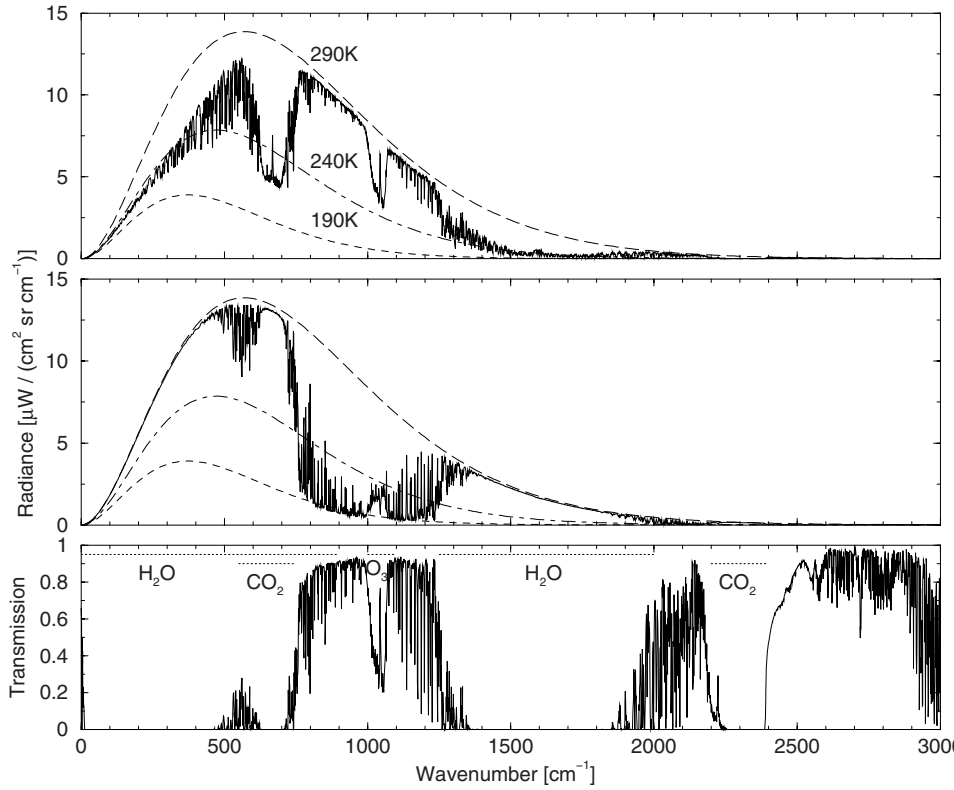

Fig. 1.5. Infrared spectrum of the Earth atmosphere: upwelling radiation seen by an observer above the atmosphere (top), downwelling radiation seen by an observer at sealevel (middle) and atmospheric transmission for a vertical path (bottom). The blackbody radiation according to Planck's function for three representative values and the main absorption bands are indicated too.

In summary, the spectral absorption or emission characteristics combined with monotonically increasing path length allows a mapping between altitude and wavelength, thus providing a direct link between absorber amount or temperature and observed radiation.

1.3 Radiative transfer

In atmospheric remote sensing, the radiation seen by an observer is described by the theory of radiative transfer with an appropriate instrument model. Before discussing radiative transfer models for the UV/vis and IR/mw spectral ranges, we define some quantities of central importance. For a thorough discussion of the material presented in this section we recommend classical textbooks on atmospheric radiation as for example, Goody and Yung (1989), Thomas and Stamnes (1999), Liou (2002), and Zdunkowski et al. (2007).

1.3.1 Definitions

Different variables are used to characterize the 'color' of electromagnetic waves: wavelength λ with units μm, nm, or Å are common in the ultraviolet and visible range, wavenumbers $\nu = 1/\lambda$ in units of cm^{-1} are used in the infrared, and frequencies $\tilde{\nu} = c\nu$ (with c being the speed of light) are employed in the microwave regime. Numerically one has $\nu\,[\mathrm{cm}^{-1}] = 10\,000/\lambda\,[\mu\mathrm{m}] \approx 30\tilde{\nu}\,[\mathrm{GHz}]$.

Monochromatic radiance or intensity is defined as the differential amount of energy $\mathrm{d}E_\lambda$ in a given wavelength interval $(\lambda, \lambda + \mathrm{d}\lambda)$ crossing an area $\mathrm{d}A$ into a solid angle $\mathrm{d}\Omega$, oriented with an angle θ relative to the normal $\mathbf{n}$ of the area, within a time interval $\mathrm{d}t$ (Figure 1.6),

$$I_\lambda = \frac{\mathrm{d}E_\lambda}{\cos\theta\,\mathrm{d}\Omega\,\mathrm{d}t\,\mathrm{d}A\,\mathrm{d}\lambda}. \tag{1.2}$$

The definition of the radiance I_ν is done in a similar manner.

For a beam of radiation traveling in a certain direction, with distances measured by the path variable $s = |\mathbf{r}_1 - \mathbf{r}_2|$, the ratio of the radiances at two different locations defines the transmission

$$\mathcal{T}(\mathbf{r}_1, \mathbf{r}_2) = \frac{I(\mathbf{r}_1)}{I(\mathbf{r}_2)}. \tag{1.3}$$

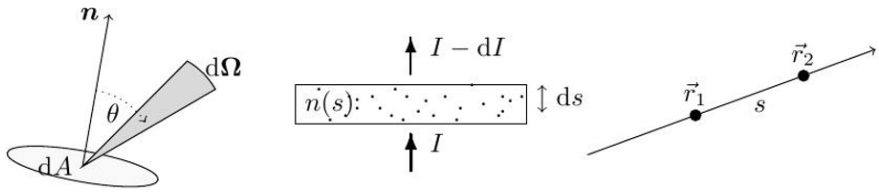

Fig. 1.6. Concepts of radiative transfer. Left: illustration of radiance definition (1.2). Middle: schematics of radiation attenuation $\mathrm{d}I$ traversing a path element $\mathrm{d}s$ with absorber density n. Right: path $s = |\mathbf{r}_1 - \mathbf{r}_2|$ relevant for the definition of optical depth and transmission.

1.3.2 Equation of radiative transfer

A beam of radiation traversing the atmosphere will be attenuated by interactions with the atmospheric constituents, and the extinction (absorption and scattering) is proportional to the amount of incoming radiation, the path distance $\mathrm{d}s$ in the direction $\mathbf{\Omega}$, and the density n of the medium, i.e., $\mathrm{d}I \propto -In\,\mathrm{d}s$ (Figure 1.6). On the other hand, the thermal emission of the medium and the scattering processes will result in an increase of the radiation energy described by a 'source function' $J(\mathbf{r}, \mathbf{\Omega})$. The total change of radiation is given by the equation of radiative transfer

$$\frac{1}{n(\mathbf{r})C_{\mathtt{ext}}(\mathbf{r})}\frac{\mathrm{d}I}{\mathrm{d}s}(\mathbf{r}, \mathbf{\Omega}) = -I(\mathbf{r}, \mathbf{\Omega}) + J(\mathbf{r}, \mathbf{\Omega}). \tag{1.4}$$

The quantity $C_{\mathtt{ext}}$ is called the extinction cross-section, and its product with the number density is the extinction coefficient $\sigma_{\mathtt{ext}} = nC_{\mathtt{ext}}$.

In the absence of any sources, the differential equation can be readily solved and we have (Beer–Lambert–Bouguer law)

$$\mathcal{T}(\mathbf{r}_1, \mathbf{r}_2) = \frac{I(\mathbf{r}_1)}{I(\mathbf{r}_2)} = \exp\left(- \int\limits_{|\mathbf{r}_1 - \mathbf{r}_2|} C_{\mathtt{ext}}(\mathbf{r})\, n(\mathbf{r})\, \mathrm{d}s \right), \tag{1.5}$$

where the integral in the exponent is the so-called (extinction) optical depth between the points $\mathbf{r}_1$ and $\mathbf{r}_2$,

$$\tau_{\mathtt{ext}}(\mathbf{r}_1, \mathbf{r}_2) = \int\limits_{|\mathbf{r}_1 - \mathbf{r}_2|} C_{\mathtt{ext}}(\mathbf{r})\, n(\mathbf{r})\, \mathrm{d}s = \int\limits_{|\mathbf{r}_1 - \mathbf{r}_2|} \sigma_{\mathtt{ext}}(\mathbf{r})\, \mathrm{d}s.$$

Equation (1.4) is a linear first-order differential equation that can be formally integrated giving

$$I(\mathbf{r}_{\mathtt{o}}, \boldsymbol{\Omega}) = I(\mathbf{r}_{\mathtt{s}}, \boldsymbol{\Omega}) \exp\big(-\tau_{\mathtt{ext}}(\mathbf{r}_{\mathtt{o}}, \mathbf{r}_{\mathtt{s}})\big) + \int\limits_{|\mathbf{r}_{\mathtt{o}} - \mathbf{r}_{\mathtt{s}}|} J(\mathbf{r}, \boldsymbol{\Omega}) \exp\big(-\tau_{\mathtt{ext}}(\mathbf{r}_{\mathtt{o}}, \mathbf{r})\big)\, \mathrm{d}s. \tag{1.6}$$

The integral form of the radiative transfer equation (1.6) describes the radiation seen by an observer at $\mathbf{r}_{\mathtt{o}}$; the first term is the source radiation at $\mathbf{r}_{\mathtt{s}}$ (e.g., Earth's surface in case of a downlooking observer) attenuated according to Beer's law (1.5) and the second term represents the radiation due to emission and scattering at intermediate points along the line of sight.

The atmospheric energy budget is essentially determined by solar insolation (roughly in the UV–vis–IR spectral range 0.2–0.35 μm) and emission by the Earth and its atmosphere (in the infrared spectral range 3.5–100 μm). For most practical purposes, these two spectral regions may be treated separately: in the solar spectral range it is justified to neglect the thermal emission of the Earth–atmosphere system, whereas in the infrared the scattering processes are usually important only in the so-called atmospheric window region 8–12.5 μm (Figure 1.5). However, as the clear atmosphere is almost transparent to the infrared radiation in this region, the atmospheric window is of minor importance for remote sensing of trace gases (except for ozone).

1.3.3 Radiative transfer in the UV

The radiation field can be split into two components: the direct radiation, which is never scattered in the atmosphere and reflected by the ground surface, and the diffuse radiation, which is scattered or reflected at least once. Neglecting the thermal emission, the source function J can be decomposed as

$$J(\mathbf{r}, \boldsymbol{\Omega}) = J_{\mathtt{ss}}(\mathbf{r}, \boldsymbol{\Omega}) + J_{\mathtt{ms}}(\mathbf{r}, \boldsymbol{\Omega}), \tag{1.7}$$

where the single and the multiple scattering source functions are given by

$$J_{\mathtt{ss}}(\mathbf{r}, \boldsymbol{\Omega}) = F \frac{\omega(\mathbf{r})}{4\pi} P(\mathbf{r}, \boldsymbol{\Omega}, \boldsymbol{\Omega}_{\mathtt{sun}})\, \mathrm{e}^{-\tau_{\mathtt{ext}}(\mathbf{r}, \mathbf{r}_{\max})},$$

and

$$J_{\mathtt{ms}}(\mathbf{r},\mathbf{\Omega}) = \frac{\omega(\mathbf{r})}{4\pi}\int_{4\pi} P(\mathbf{r},\mathbf{\Omega},\mathbf{\Omega}')\, I(\mathbf{r},\mathbf{\Omega}')\ \mathrm{d}\Omega',$$

respectively. In the above relations, $\omega = \sigma_{\mathtt{scat}}/\sigma_{\mathtt{ext}}$ is the single scattering albedo, $\sigma_{\mathtt{scat}}$ is scattering coefficient, F is the incident solar flux, P is the phase function, $\mathbf{\Omega}_{\mathtt{sun}}$ is the unit vector in the sun direction, and $\mathbf{r}_{\max}$ is the point at the top of the atmosphere corresponding to $\mathbf{r}$, that is, $\mathbf{r}_{\max} = \mathbf{r} - |\mathbf{r}_{\max} - \mathbf{r}|\,\mathbf{\Omega}_{\mathtt{sun}}$. It should be pointed out that technically, there is no absolute dividing line between the Earth's atmosphere and space, but for studying the balance of incoming and outgoing energy on the Earth, an altitude at about 100 kilometers above the Earth is usually used as the 'top of the atmosphere'.

An accurate interpretation of the measurements performed by satellite instruments in arbitrary viewing geometries requires the solution of the radiative transfer equation in a three-dimensional inhomogeneous spherical atmosphere. For this type of radiative transfer problems, the Monte Carlo technique (Marchuk et al., 1980) is a possible candidate. In a Monte Carlo simulation the radiance at the top of the atmosphere is determined statistically by simulating a large number of individual photon trajectories through the atmosphere. This method is computationally very expensive in the calculation of the backscattered radiance, because many photons are lost when they leave the atmosphere at other positions and in other directions than the one to the satellite. For atmospheric applications, the so-called backward Monte Carlo method is more efficient. Here, the photons are started from the detector and their path is followed backward to the point where they leave the atmosphere in solar direction. The disadvantages of this method are, however, its poor accuracy for optically thick or weakly absorbing media, and that for each viewing geometry, a new backward calculation has to be performed. Additionally, the required linearization of such Monte Carlo models is a challenging task. Applications of the Monte Carlo method for radiance calculations in a spherical atmosphere can be found in Oikarinen et al. (1999).

Radiative transfer models

In practice, simplified radiative transfer models are used to simulate the radiances at the observer's position and in the direction of the instrument line-of-sight. These can be categorized depending on the assumptions made for the geometry of the model atmosphere.

Plane-parallel radiative transfer calculations have been applied successfully for nadir measurements with solar zenith angles up to 75°. The discrete ordinate method (Stamnes et al., 1988), the doubling-adding method (Hansen, 1971), the finite difference method (Barkstrom, 1975) and the Gauss–Seidel iteration method (Herman and Browning, 1965) have been used to solve the radiative transfer equation in a plane-parallel atmosphere. Further details on the mentioned solution methods can be found in Lenoble (1985).

For nadir viewing geometries with large solar zenith angles and for limb viewing geometries, the so-called *pseudo-spherical approximation* has been developed (Dahlback and Stamnes, 1991). In this approximation, the single scattering radiance is computed in a spherical atmosphere, whereas the multiple scattering radiance is still calculated in a plane-parallel geometry. For limb measurements, the effect of a varying solar zenith angle along the line of sight is accounted for by performing a set of independent pseudo-spherical calculations for different values of the solar zenith angle. This model is equivalent to the *independent pixel approximation* for three-dimensional radiative transfer in clouds, and

can be regarded as a first-order spherical correction to the plane-parallel formulation of the radiative transfer. Solution methods for radiative transfer in a pseudo-spherical atmosphere include the discrete ordinate method (Spurr, 2001, 2002), the finite difference method (Rozanov et al., 2000), and the discrete ordinate method with matrix exponential (Doicu and Trautmann, 2009a).

For a subhorizon Sun as well as for lines of sight with large tangent heights, the independent pixel approximation leads to errors of about 4%. For such problems, the *spherical shell approximation* (Rozanov et al., 2001; Walter et al., 2005; Doicu and Trautmann, 2009e) delivers more accurate results. Here, the atmosphere is approximated by homogeneous spherical shells and no horizontal inhomogeneities in the optical parameters are considered. The radiative transfer equation is solved by means of a Picard iteration with a long or a short characteristic method (Kuo et al., 1996).

Accurate simulations of radiances in ultraviolet and visible spectral regions should take into account that light scattered by the atmosphere is polarized and that approximately 4% of molecular scattering is due to the inelastic rotational Raman component.

Polarization

The radiation and state of polarization of light can be described by the Stokes vector $\mathbf{I} = [I, Q, U, V]^T$, where I is the radiance, Q is a measure for the polarization along the x- and y-axis of the chosen reference frame, U is a measure of the polarization along the $+45^\circ$ and -45° directions, and V describes the circular polarization. The vector radiative transfer equation reads as

$$\frac{\mathrm{d}\mathbf{I}}{\mathrm{d}s}\left(\mathbf{r},\boldsymbol{\Omega}\right) = -\sigma_{\mathtt{ext}}\left(\mathbf{r}\right)\mathbf{I}\left(\mathbf{r},\boldsymbol{\Omega}\right) + \sigma_{\mathtt{ext}}\left(\mathbf{r}\right)\mathbf{J}\left(\mathbf{r},\boldsymbol{\Omega}\right),$$

where $\mathbf{J}$ is the source term. As in the scalar case, the source function can be split into a single and a multiple scattering component, and we have the representations

$$\mathbf{J}_{\mathtt{ss}}\left(\mathbf{r},\boldsymbol{\Omega}\right) = F\frac{\omega\left(\mathbf{r}\right)}{4\pi}\,\mathrm{e}^{-\tau_{\mathtt{ext}}\left(\mathbf{r},\mathbf{r}_{\max}\right)}\mathbf{Z}\left(\mathbf{r},\boldsymbol{\Omega},\boldsymbol{\Omega}_{\mathtt{sun}}\right)\begin{bmatrix}1\\0\\0\\0\end{bmatrix},$$

and

$$\mathbf{J}_{\mathtt{ms}}\left(\mathbf{r},\boldsymbol{\Omega}\right) = \frac{\omega\left(\mathbf{r}\right)}{4\pi}\int_{4\pi}\mathbf{Z}\left(\mathbf{r},\boldsymbol{\Omega},\boldsymbol{\Omega}'\right)\mathbf{I}\left(\mathbf{r},\boldsymbol{\Omega}'\right)\,\mathrm{d}\Omega',$$

with $\mathbf{Z}$ being the phase matrix.

The instrumental signal should be simulated with a vector radiative transfer model for two reasons.

First, light reflected from Earth's atmosphere is polarized because of (multiple) scattering of unpolarized light by air molecules and aerosols. Simulations of radiance measurements by a scalar approximation for atmospheric radiative transfer leads to errors of about 10% depending mainly on the viewing scenario (Mishchenko et al., 1994). The scalar radiative transfer errors are small in the spectral regions in which mainly single scattering takes place and significant in the spectral regions in which the amount of multiple scattering

increases because of decreasing gas absorption. For a pseudo-spherical atmosphere, vector radiative transfer models employing the discrete ordinate method (Spurr, 2006, 2008), the successive order of scattering technique (McLinden et al., 2002a) and the discrete ordinate method with matrix exponential (Doicu and Trautmann, 2009b) have been developed. A survey of vector radiative transfer models for a plane-parallel atmosphere can be found in Hansen and Travis (1974).

Second, the different optical devices in the instrument are sensitive to the state of polarization of the incident light. As a result, the radiance that is measured by the detectors, referred to as the polarization-sensitive measurement, is different to the radiance that enters in the instrument. In the calibration process, the instrumental signal is corrected for the polarization sensitivity, whereas the polarization correction factor is determined from broadband on-ground measurements. However, in spectral regions where the state of polarization is varying rapidly with wavelength, the polarization correction is not sufficiently accurate and severely influences the retrieval. To eliminate this drawback, the polarization-sensitive measurement together with the transport of radiation in the atmosphere have been simulated by means of vector radiative transfer models (Hasekamp et al., 2002; McLinden et al., 2002b).

Ring effect

The filling-in of solar Fraunhofer lines in sky spectra and the telluric filling-in of trace gas absorption features in ultraviolet and visible backscatter spectra are known as the Ring effect. Several studies (Kattawar et al., 1981; Joiner et al., 1995) have demonstrated that the main process responsible for the Ring effect is the rotational Raman scattering by molecular O_3 and N_2. In backscatter spectra, the Ring effect shows up as small-amplitude distortion, which follows Fraunhofer and absorption lines. For an inelastically scattering atmosphere, the radiative transfer equation includes an additional source term, the Raman source function, and the single and multiple scattering source terms have to be modified accordingly. Several radiative transfer models have been used to simulate the so-called Ring spectrum defined as the ratio of the inelastic and the elastic scattering radiances. These models include a Monte Carlo approach (Kattawar et al., 1981), a successive order of scattering method (Joiner et al., 1995) and a model which treats rotational Raman scattering as a first-order perturbation (Vountas et al., 1998; Landgraf et al., 2004; Spurr et al., 2008).

As Ring structures appear in the polarization signal, a complete simulation of the polarization-sensitive measurement requires a vector radiative transfer model which simulates Ring structures for all relevant Stokes parameters (Aben et al., 2001; Stam et al., 2002; Landgraf et al., 2004). The calculation of Ring spectra with a vector radiative transfer model is numerically expensive and approximation methods are desirable for large data sets. The numerical analysis performed in Landgraf et al. (2004) reveals that

(1) the polarization Ring spectra of Q and U are much weaker than those of the radiance I due to the low polarization of Raman scattered light;
(2) the combination of both a vector radiative transfer model, simulating the Stokes vector for an elastic scattering atmosphere, and a scalar radiative transfer approach, simulating the Ring spectrum for the radiance is sufficiently accurate for gas profile retrievals but not for applications involving the retrieval of cloud properties.

1.3.4 Radiative transfer in the IR and microwave

Neglecting scattering and assuming local thermodynamical equilibrium, the source function J is given by the Planck function at temperature T,

$$B(\nu, T) = \frac{2hc^2\nu^3}{\exp\left(\dfrac{hc\nu}{k_{\mathtt{B}}T}\right) - 1}. \tag{1.8}$$

The formal solution (1.6), describing the radiance I at wavenumber ν received by an instrument at position $\mathbf{r}_{\mathtt{o}}$, is given by the Schwarzschild equation

$$I(\nu, \mathbf{r}_{\mathtt{o}}) = I(\nu, \mathbf{r}_{\mathtt{s}})\mathcal{T}\left(\nu, \mathbf{r}_{\mathtt{o}}, \mathbf{r}_{\mathtt{s}}\right) + \int_{|\mathbf{r}_{\mathtt{o}} - \mathbf{r}_{\mathtt{s}}|} B\left(\nu, T(\mathbf{r})\right) \frac{\partial \mathcal{T}}{\partial s}\left(\nu, \mathbf{r}_{\mathtt{o}}, \mathbf{r}\right) \mathrm{d}s, \tag{1.9}$$

where $I(\nu, \mathbf{r}_{\mathtt{s}})$ is the background contribution at position $\mathbf{r}_{\mathtt{s}}$. The monochromatic transmission is computed according to Beer's law as

$$\mathcal{T}\left(\nu, \mathbf{r}_{\mathtt{o}}, \mathbf{r}\right) = \exp\left(-\int_{|\mathbf{r}_{\mathtt{o}} - \mathbf{r}|} \sigma_{\mathtt{abs}}(\nu, \mathbf{r}')\, \mathrm{d}s'\right) \tag{1.10}$$

$$= \exp\left(-\int_{|\mathbf{r}_{\mathtt{o}} - \mathbf{r}|} \mathrm{d}s' \sum_m C_{\mathtt{abs}m}\left(\nu, p\left(\mathbf{r}'\right), T\left(\mathbf{r}'\right)\right) n_m\left(\mathbf{r}'\right)\right). \tag{1.11}$$

Here, $\sigma_{\mathtt{abs}}$ is the absorption coefficient, p is the atmospheric pressure, n_m is the number density of molecule m, and $C_{\mathtt{abs}m}$ is its absorption cross-section.

In general, the molecular absorption cross-section is obtained by summing over the contributions from many lines. For an individual line at position $\hat{\nu}$, the cross-section is the product of the temperature-dependent line strength $S(T)$ and a normalized line shape function $g(\nu)$ describing the broadening mechanism(s), that is,

$$C_{\mathtt{abs}m}\left(\nu, p, T\right) = \sum_l S_{ml}\left(T\right) g\big(\nu, \hat{\nu}_{ml}, \gamma_{ml}\left(p, T\right)\big). \tag{1.12}$$

In the atmosphere, the combined effect of pressure broadening, corresponding to a Lorentzian line shape (indices m and l denoting molecule and line will be omitted for simplicity)

$$g_{\mathtt{L}}(\nu, \hat{\nu}, \gamma_{\mathtt{L}}) = \frac{1}{\pi} \frac{\gamma_{\mathtt{L}}}{(\nu - \hat{\nu})^2 + \gamma_{\mathtt{L}}^2}\,, \tag{1.13}$$

and Doppler broadening, corresponding to a Gaussian line shape

$$g_{\mathtt{D}}(\nu, \hat{\nu}, \gamma_{\mathtt{D}}) = \frac{1}{\gamma_{\mathtt{D}}} \left(\frac{\log 2}{\pi}\right)^{\frac{1}{2}} \exp\left(-\log 2 \left(\frac{\nu - \hat{\nu}}{\gamma_{\mathtt{D}}}\right)^2\right), \tag{1.14}$$

can be represented by a convolution, i.e., the Voigt line profile $g_{\mathtt{V}} = g_{\mathtt{L}} \otimes g_{\mathtt{D}}$. Pressure broadening (air-broadening, with self-broadening neglected) and Doppler broadening half-widths are given by

$$\gamma_{\mathtt{L}}(p, T) = \gamma_{\mathtt{L}0} \frac{p}{p_{\mathtt{ref}}} \left(\frac{T_{\mathtt{ref}}}{T}\right)^{\alpha}$$

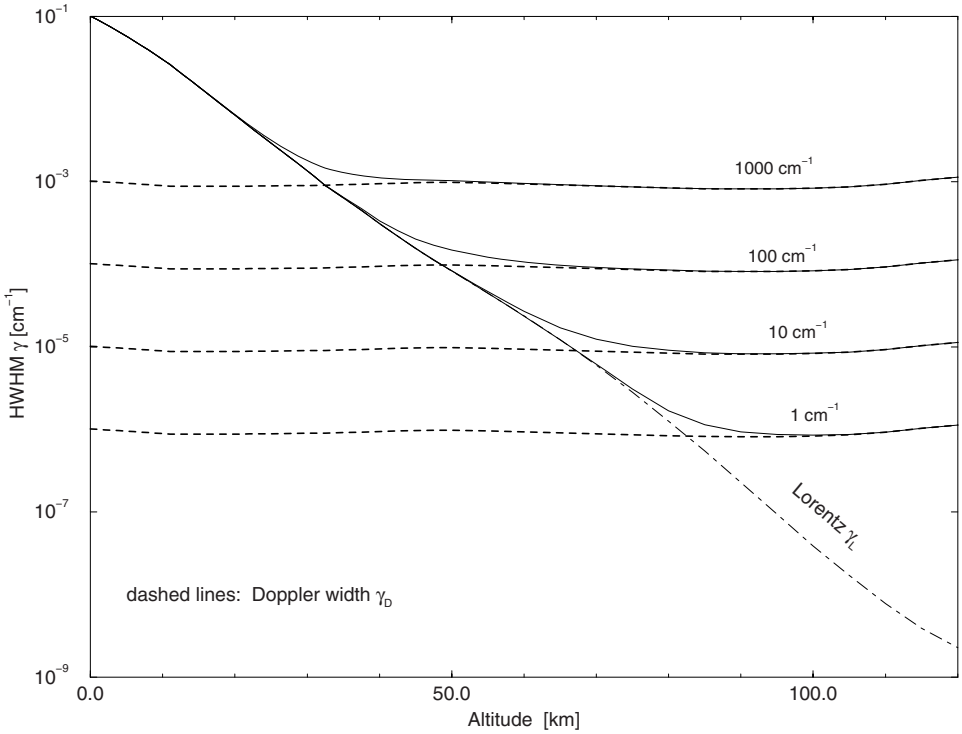

Fig. 1.7. Lorentz, Gauss and Voigt half-widths (HWHM) as a function of altitude in the Earth atmosphere for a variety of line positions $\hat{\nu}$. Pressure and temperature are from US Standard Atmosphere and the molecular mass is 36 amu.

and

$$\gamma_{\mathrm{D}}(T) = \hat{\nu}\sqrt{2\log 2\frac{k_{\mathrm{B}}T}{mc^2}},$$

respectively. Here, $p_{\mathtt{ref}}$ and $T_{\mathtt{ref}}$ are the reference pressure and temperature of line parameters, respectively, m denotes the molecular mass, and α describes the temperature dependence of pressure broadening. Note that pressure broadening dominates in the lower atmosphere; the transition altitude, where Doppler broadening becomes important, moves up from the middle stratosphere to the mesosphere with increasing wavelength (Figure 1.7).

Spectroscopic line parameters required for the calculation of the molecular absorption cross-sections, e.g., the line position $\hat{\nu}$, the line strength S, the temperature exponent α, the air-broadening half-width $\gamma_{\mathrm{L}0}$, and the lower state energy E (required to calculate $S\,(T)$ from the database entry $S\,(T_{\mathtt{ref}})$) have been compiled in various databases such as HITRAN (HIgh-resolution TRANsmission molecular absorption database), GEISA (Gestion et Etude des Informations Spectroscopiques Atmosphériques) and JPL (Jet Propulsion Laboratory) catalog. The latest versions of HITRAN (Rothman et al., 2009) and GEISA (Jacquinet-Husson et al., 2008) list parameters of some million transitions for several dozen molecules from the microwave ($\hat{\nu} = 10^{-6}$ cm^{-1}) to the ultraviolet ($\hat{\nu} \approx 25\,232$

and $\hat{\nu} \approx 35\,877\ \mathrm{cm}^{-1}$, respectively), whereas the JPL catalogue (Pickett et al., 1998) covers millions of rotational transitions in the microwave regime.

At a first glance the forward model appears to be much easier to solve in the infrared than in the ultraviolet as the source function is known. However, for high resolution atmospheric spectroscopy, the line-by-line (lbl) computation of (1.9) and (1.10) remains a challenging task because thousands of spectral lines have to be included in the sum (1.12). Moreover, as the monochromatic wavenumber grid point spacing determined by the half-widths of the spectral lines (cf. Figure 1.7) is very fine, accurate modeling of the spectrum may require thousands or even millions of spectral grid points. Finally, the convolution integral defining the Voigt line profile cannot be solved analytically, and numerical approximations have to be used.

In view of the computational challenges of lbl-modeling, alternative approaches have been used for low to moderate resolution spectra. Band models have been developed since the early days of radiative transfer modeling in meteorology and astrophysics (Goody and Yung, 1989; Liou, 2002; Thomas and Stamnes, 1999; Zdunkowski et al., 2007). More recently, the k-distribution and correlated k methods (Fu and Liou, 1992; Lacis and Oinas, 1991) or exponential sum fitting (Wiscombe and Evans, 1977) have been utilized.

Scattering is usually ignored in lbl models. However, if the analysis of data provided by spaceborne infrared sounders would be confined to clear sky observations only, a large fraction of data would be ignored. For nadir sounding, single scattering can be implemented with moderate effort, but multiple scattering, especially for limb sounding geometries, is still a challenging task. Various attempts have been described by Emde et al. (2004), Höpfner et al. (2002), Höpfner and Emde (2005), and Mendrok et al. (2007).

Intercomparisons of high-quality (laboratory and atmospheric) infrared spectra have revealed discrepancies with accurate model spectra obtained with the lbl approach (1.12). These deviations are commonly attributed to the so-called 'continuum', and a variety of explanations have been given in the literature, e.g., deviations of the far wing line profile from the Lorentzian line shape, contributions from water dimers $(H_2O)_2$ etc. For modeling infrared and microwave spectra, the semi-empirical approach developed by Clough et al. (1989) is widely used (see also Clough et al., 2005), whereas the empirical corrections due to Liebe et al. (1993) are frequently employed in the microwave regime.

When local thermodynamic equilibrium (LTE) is assumed, a local temperature can be assigned everywhere in the atmosphere, and thermal emission can be described by Planck's law of blackbody radiation (1.8). However, because temperature and radiation vary in space and time, the atmosphere is not in thermodynamic equilibrium. Nevertheless, the LTE assumption is justified in the troposphere and stratosphere, where the density of air is sufficiently high so that the mean time between molecular collisions is much smaller than the mean lifetime of an excited state of a radiating molecule. Thus, equilibrium conditions exist between vibrational, rotational and translation energy of the molecule. The breakdown of LTE in the upper atmosphere implies that the source function is no longer given by the Planck function. An adequate description of collisional and radiative processes under non-LTE conditions requires quantum theoretical considerations; see Lopez-Puertas and Taylor (2001) for an in-depth treatment.

1.3.5 Instrument aspects

In general, the finite resolution of the spectrometer results in a modification or smearing of the 'ideal' spectrum. This effect can be modeled by a convolution of the 'monochromatic' spectrum $S_{\mathtt{mc}}(\nu)$ (radiance I or transmission $\mathcal{T}$) with an instrument line shape function ILS (also termed spectral response function SRF),

$$S_{\mathtt{obs}}(\nu) = \int_{-\infty}^{\infty} ILS\left(\nu - \nu'\right) S_{\mathtt{mc}}\left(\nu'\right) \mathrm{d}\nu'. \tag{1.15}$$

The function ILS clearly depends on the type of the instrument; a Gaussian can be used as a first approximation in many cases, e.g., for a grating instrument. For a Fourier transform spectrometer such as MIPAS (Michelson Interferometer for Passive Atmospheric Sounding) or IASI (Infrared Atmospheric Sounding Interferometer), the finite optical path difference L of the Michelson interferometer corresponds to a multiplication of the interferogram with a box function, so that (to a first approximation) the line shape function is given by

$$ILS\left(\nu - \nu'\right) = 2L\,\mathrm{sinc}\left(2\pi L\left(\nu - \nu'\right)\right) = \frac{\sin\left(2\pi L\left(\nu - \nu'\right)\right)}{\pi\left(\nu - \nu'\right)}. \tag{1.16}$$

On the other hand, the finite aperture of an instrument results in a superposition of ideal 'pencil beam' spectra corresponding to an infinitesimal field of view. Modeling of this finite field of view is especially important for limb geometry and can be done by convolving the pencil-beam spectra with a field-of-view function. Frequently, this function is approximated by box, triangular, or Gauss functions.

1.3.6 Derivatives

Often, the radiative transfer models are optimized to deliver in addition to the simulated radiance, the partial derivatives of the radiance with respect to the atmospheric parameters being retrieved. The process of obtaining the set of partial derivatives, which constitute the Jacobian matrix, is commonly referred to as linearization analysis. Several techniques for performing a linearization analysis can be distinguished

In many cases, the Jacobian matrix is computed by *finite differences*, and this calculation is the most time-consuming part of the retrieval. Even more serious is the fact that the amount of perturbation is difficult to predict and an improper choice leads to truncation and/or cancellation errors; see Gill et al. (1981) for a pertinent discussion.

Analytical calculation of derivatives is advantageous, both for computational efficiency and accuracy. From (1.6) it is apparent that the partial derivatives of the radiance measured by the instrument are given by the partial derivatives of the single and the multiple scattering radiances. As the multiple scattering radiance depends on the solution of the radiative transfer equation, derivatives calculation can be performed by linearizing the radiative transfer equation with respect to the desired parameters. A linearized radiative transfer model based on an analytical determination of the partial derivatives of the conventional discrete ordinate solution for radiance has been developed by Spurr (2001, 2002, 2008), while a linearized forward approach based on the discrete ordinate method with

matrix exponential has been proposed in Doicu and Trautmann (2009d). For infrared applications, analytic derivatives are implemented in the codes ARTS (Bühler et al., 2005), KOPRA (Stiller et al., 2002) and MOLIERE (Urban et al., 2004). However, calculating the derivatives manually and implementing these in a moderately large code as required for general-purpose radiative transfer is tedious and error-prone. Moreover, no automatic updates of the derivatives calculation in the case of upgrades of the forward model are available.

The measured radiance can be expressed in the framework of a *forward-adjoint approach* as the scalar product of the solution of the adjoint problem and the source function of the forward problem. Employing the linearization technique to the forward and the adjoint problems, analytical expressions for the derivatives in a plane-parallel atmosphere have been derived in Marchuk (1964, 1995), Box (2002), Ustinov (2001, 2005), Rozanov and Rozanov (2007), and Landgraf et al. (2001). For a pseudo-spherical atmosphere, this approach has been applied to nadir viewing geometries in Walter et al. (2004) and to limb geometries in Ustinov (2008), and Doicu and Trautmann (2009c). The forward-adjoint approach is extremely efficient because only two radiative transfer calculations are required for derivative calculations. In this context, Landgraf et al. (2001) reported that under certain conditions a forward-adjoint approach based on the Gauss–Seidel iteration technique is approximately a factor of 20–30 faster than a linearized forward approach based on the conventional discrete ordinate solution.

Automatic or algorithmic differentiation provides a pleasant alternative to quickly generate derivative-enhanced versions of computer codes. Automatic differentiation techniques (Griewank and Corliss, 1991; Griewank, 2000) are based on the observation that every model implemented as a computer program is essentially formulated in terms of elementary mathematical operations (sums, products, powers) and elementary functions. In contrast to integration, differentiation is based on a few simple recipes such as the chain rule, and these can be performed automatically by some kind of precompiler, taking a computer code of the forward model as input and delivering a code that additionally produces derivatives with respect to some chosen variables. A number of automatic differentation tools are available for Fortran and C (cf. the compilation given at http://www.autodiff.org/). This approach has been used by Schreier and Schimpf (2001), and Schreier and Boettger (2003) to implement Jacobian matrices in an infrared line-by-line radiative transfer code.

1.4 Inverse problems

In atmospheric remote sensing, the relationship between the state parameters x and collected observations making up some set of data y is described by a forward model F. This encapsulates a radiative transfer model and an instrument model, and formally, we write

$$y = F(x).$$

The task of computing the data y given the state parameters x is called the forward problem, while the mathematical process to compute x given y is called the inverse problem (Figure 1.8). Atmospheric remote sensing deals with the inverse problem. In fact, inverse problems are ubiquitous challenges in almost any field of science and engineering, from astrophysics, helioseismology, geophysics, quantum mechanical scattering the-

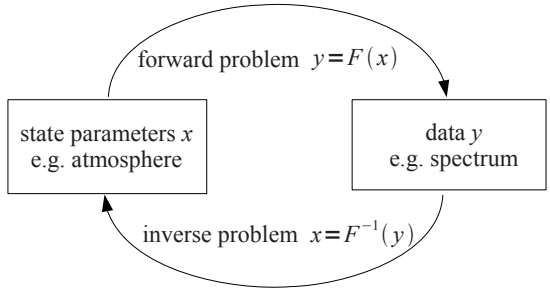

Fig. 1.8. Forward and inverse problem.

ory and material science to medicine with its large diversity of imaging and tomographic techniques, see, for example, Craig and Brown (1986), Groetsch (1993), Wing (1991) for some introductory surveys, and Baumeister (1987), Engl et al. (2000), Hansen (1998), Kaipio and Somersalo (2005), Kaltenbacher et al. (2008), Kirsch (1996), Menke (1984), Parker (1994), Rieder (2003), Tarantola (2005), Vogel (2002) for more advanced treatments. Inverse problems for atmospheric remote sensing are discussed by Twomey (1977), Stephens (1994) and Rodgers (2000).

The forward model is closely connected with the actual observation being performed and mirrors the physics of the measurement process. In contrast the approach to solving the inverse problem is (to some extent) independent of the physical process and the methods developed throughout this book can be used for inverse problems in other fields as well.

In a general framework, the data y may be a function of frequency (or wavelength) or it may be a collection of discrete observations. In the first case, the problem is called a continuous problem, while in the second case it is called a semi-discrete problem. When both x and y are discrete, the corresponding problem is a discrete problem. In order to avoid possible confusions, vectors will be denoted by bold letters, e.g., $\mathbf{x}$ is a vector of state parameters or simply a state vector, while x is a state parameter function. As any measurement system can deliver only a discrete, finite set of data, the problems arising in atmospheric remote sensing are semi-discrete. Moreover, due to the complexity of the radiative transfer, the forward model has to be computed by a numerical algorithm, which, in turn, requires a discretization of the state parameter function. For these reasons, the atmospheric inverse problems we are dealing with are discrete.

An important issue is that actual observations contain instrumental or measurement noise. We can thus envision data $\mathbf{y}^\delta$ as generally consisting of noiseless observations $\mathbf{y}$ from a 'perfect' instrument plus a noise component $\boldsymbol{\delta}$, i.e.,

$$\mathbf{y}^\delta = \mathbf{y} + \boldsymbol{\delta}.$$

For limb viewing geometries, $\mathbf{y}^\delta$ is usually a concatenation of spectra corresponding to all limb scans, and the reconstruction of atmospheric profiles from a limb-scanning sequence of spectra is known as the global-fit approach (Carlotti, 1988).

The radiation seen by an observer depends on a large variety of parameters, i.e., spectral range, observation geometry, instrument settings, optical properties of the atmospheric constituents, and the state of the atmosphere characterized by pressure, temperature, and

concentration of molecules and particles. For a complete and accurate modeling of the measurement process, the forward model has to take into account all relevant parameters. However, only a single or a few variables of the atmospheric system can usually be retrieved from the observed data, and all other parameters are assumed to be known. For this reason and following Rodgers (2000), we split the state vector $\mathbf{x}$ into two components: the first component $\mathbf{x}_1$ represents the atmospheric profile (temperature or concentration profile of one particular species of interest) to be retrieved, while the second component $\mathbf{x}_2$ includes all auxiliary parameters or model parameters, which influence the retrieval. It is a common practice to retrieve atmospheric profiles individually in sequence, where the sequence of the target species and temperature retrieval is determined according to the degree of their reciprocal interference. The auxiliary parameters may include

- surface parameters (surface albedo, ground emissivity factor),
- spectral corrections due to the instrumental convolution process (tilt, undersampling, polarization spectra),
- instrumental parameters (pointing offset, wavelength shift and squeeze, ILS parameters, baseline shift),
- atmospheric continuum (including all absorption that varies smoothly with the frequency and being represented by a polynomial),
- parameters describing complex physical processes (Ring spectrum, non-LTE/LTE population ratio, temperature and volume mixing ratio gradients).

In general, the auxiliary parameters can be retrieved together with the main atmospheric profile, they can be treated as an observation uncertainty, or they can be assumed to be perfectly known. In the first case, we are talking about a multi-parameter problem, while in the second case, we employ the so-called marginalizing method to solve the inverse problem. Another option is to perform the retrieval in two stages (Rozanov et al., 2005). In the first stage, also known as the pre-processing stage, the scaling factors of the spectral corrections are computed together with the shift and squeeze corrections by considering a linearization of the forward model about a reference state. In the second stage, referenced to as the inversion stage, the scaling factors determined in the pre-processing step are used to compute the corrected measured spectra, and the nonlinear problem is solved for the trace gas profile.

In fact, the true physics of the measurement is described by the so-called forward function $\mathbf{f}(\mathbf{x})$ (Rodgers, 2000). The forward function is difficult to compute because the real physiscs is far too complex to deal with explicitly. For example, the correct modeling of aerosol and cloud particles with respect to their shape, size distribution and loading is an impossible task. The forward model errors $\boldsymbol{\delta}_{\mathtt{m}}$, defined through the relation

$$\mathbf{f}(\mathbf{x}) = \mathbf{F}(\mathbf{x}) + \boldsymbol{\delta}_{\mathtt{m}},$$

are difficult to compute and only the norm $\|\boldsymbol{\delta}_{\mathtt{m}}\|$ can be estimated by an additional computational step.

To get a first idea about the difficulties associated with the solution of inverse problems, we consider an elementary example. Let $x(z)$ be some function defined on the interval $[0, z_{\max}]$, and let us compute the integral $y(z) = \int_0^z x(t)\,\mathrm{d}t$. Evidently, y is an antiderivative of x, and so, the original function can be rediscovered by taking the derivative of y, that is, $x(z) = y'(z)$. Formally, the integration step is the forward problem,

while the differentiation step is the inverse problem. Now, let y^δ be a perturbation of y. Then, the derivative calculation $x^\delta(z) = y^{\delta\prime}(z)$ is an unstable process because, as the opposite of the smoothing effect of integration, differentiation is very sensitive to small perturbations of the function. As a result, x^δ may deviate significantly from x, even though y^δ is close to y.

The goal of this book is to present numerical (regularization) methods for inverse problems involving the reconstruction of atmospheric profiles from (satellite) measurements. The solution of atmospheric inverse problems is not an easy task due to the so-called ill-posedness of the equation describing the measurement process. This concept will be clarified in the next chapter.